Physics Procedia

Volume 75, 2015, Pages 932–938

20th International Conference on Magnetism

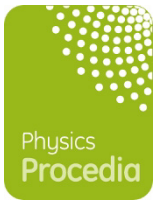

Longitudinal Spin Seebeck Effect in Bi-substituted Neodymium Iron Garnet on Gadolinium Gallium Garnet Substrate Prepared by MOD Method

H. Asada[1], A. Kuwahara[1], K. Sueyasu[1], T. Ishibashi[2], Q. Liu[2], G. Lou[2], K. Kishimoto[1], T. Koyanagi[1]

[1]*Department of Electronic Devices Engineering, Graduate School of Science and Engineering, Yamaguchi University, Ube 755-8611, Japan*

[2]*Department of Materials Science and Technology, Nagaoka University of Technology, Nagaoka, 940-2188, Japan*

asada@yamaguchi-u.ac.jp

Abstract

Bi-substituted Neodymium Iron Garnet ($Nd_{3-x}Bi_xFe_5O_{12}$, Bi:NIG) thin films with the Bi composition x=0-1.0 are prepared on both the (001) and (111) oriented gadolinium gallium garnet (GGG) substrates by a metal organic decomposition method. Crystalline qualities and magnetic properties of these films are examined by X-ray diffraction, atomic force microscopy and vibrating sample magnetometer. Longitudinal spin Seebeck effects (LSSEs) are investigated by means of the inverse spin Hall effect in a Pt film. The increase of LSSE voltage in Bi:NIG(x=0-1.0)/Pt bilayers on GGG(001) is observed with the increase of Bi composition. In the case of GGG(111), the LSSE voltage for Bi:NIG(x=1.0) is also larger than that for NIG.

Keywords: spin-Seebeck, garnet ferrite, metal-organic decomposition method, spin caloritronics

1 Introduction

The spin Seebeck effect (SSE) enables a new thermoelectric device utilizing the spin current generated by the temperature gradient[1]. The conventional Seebeck effect (SE) is observed only in electric conductors. A decrease in the thermal conductivity and an increase in the electrical conductivity of thermoelectric materials are needed to improve the conversion efficiency but these properties contradict each other. Unlike the conventional SE, the SSE is observed in ferromagnetic insulators as well as the metals and semiconductors since the spin current is also carried by magnon [1-8]. Spin-thermoelectric coating based on a longitudinal SSE (LSSE) has been demonstrated using $Y_2BiFe_5O_{12}$ (Bi:YIG) films formed by a metal-organic decomposition (MOD) method [9]. Compared with

Selection and peer-review under responsibility of the Scientific Programme Committee of ICM 2015

doi:10.1016/j.phpro.2015.12.128

conventional thermoelectric devices, the spin-thermoelectric coating has the quite simple structure which consists of two layers of paramagnetic metal and ferromagnetic insulator coated on a heat source. So far, the LSSE of the ferromagnetic insulator has been mainly investigated in yttrium based iron garnets. It is important for the practical application to increase the thermal-to-electric conversion efficiency in LSSE devices. In order to obtain the guidance for material development and physical understanding, the systematic study for various materials is effective. We have reported the Ga composition dependence of LSSE voltage in $Nd_2BiFe_{5-x}Ga_xO_{12}$/Pt bilayer [10]. Faraday rotation in Bi-substituted iron garnets enhanced by increasing amount of Bi due to the larger spin-orbit interaction. Since Nd^{3+} has similar ionic radius (99 pm) with Bi^{3+} (102 pm), Bi can be highly substituted in NIG from the view point of the crystalline quality [11,12]. It has been reported that the LSSE voltage in a YIG/Pt system is very sensitive to the interface condition of the YIG [13].

In this study, we prepare $Nd_{3-x}Bi_xFe_5O_{12}$ (Bi:NIG) thin films with the Bi composition x=0-1.0 by using the MOD method on the (001) oriented gadolinium gallium garnet (GGG) substrates. The measurements of the electric voltage caused by the SSE in Bi:NIG/Pt bilayers are conducted using the longitudinal configuration. NIG and Bi:NIG(x=1.0) films are also prepared on (111) oriented GGG and the LSSE voltages are measured.

2 Experiments

Bi:NIG films were prepared using MOD solutions which were consisting of solutions made from carboxylates with desired chemical compositions [14]. The MOD method is advantageous to obtain high quality garnet films over a wide area at low cost because of its simple fabrication process; spin-coating and annealing of the MOD solution. After spin-coating of the MOD solutions on GGG substrates (GGG thickness=0.5 mm), sample was dried at 100 °C for 10 min and was pre-annealed at 450 °C for 10 min using a hot-plate. These processes were repeated 5 times and the expected film thickness from the concentration of carboxylates was approximately 200 nm. Subsequently, samples were annealed for crystallization in a furnace at 700 °C for 13 h in air. Finally, a 10-nm-thick Pt film was deposited by using ultra-high-vacuum magnetron sputtering system on the Bi:NIG films with a size of 10×5 mm^2. The length l and width w of Pt layer were 7 and 1 mm, respectively. As illustrated in Fig.1, a temperature gradient ∇T was created perpendicular to the film plane by sandwiching the BI:NIG/Pt bilayer between two Cu plates and an external magnetic field was applied in the film plane. Temperature difference ΔT which was measured between the Cu plates using thermocouples was set to be 10 K in this study. It was confirmed that the LSSE voltage increased almost lineally with increasing ΔT till 10 K.

3 Results and discussion

X-ray diffraction (XRD) measurements with the angle 2θ from 20 to 65 degree were carried out. It was confirmed that all films on both the (001) and (111) oriented GGG are highly oriented. Figure 2

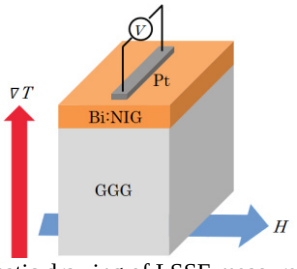

Fig.1 Schematic drawing of LSSE measurement setup.

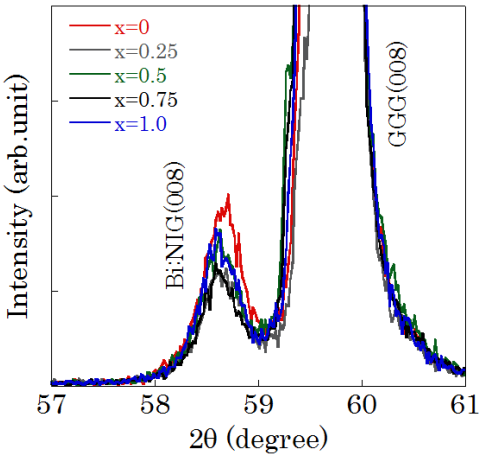

Fig.2 XRD patterns around 008 diffraction peak for Bi:NIG(x=0-1.0) films on GGG(001).

shows XRD patterns around 008 diffraction peak for the Bi:NIG (x=0, 0.25, 0.5, 0.75 and 1.0) films prepared on GGG(001), respectively. The only 008 diffraction peaks are observed close to the 008 peak of the GGG substrate. The similar peak positions, that is the similar lattice constant, is attributed to the similarity of ionic radii of Bi^{3+} and Nd^{3+}. The peak intensities for the Bi-substituted NIG films, especially with x=0.25 and 0.75, are slightly small compared to that for the pure NIG film.

The surface morphology was examined by atomic force microscopy. Topographic views of the surface of (a) NIG and (b) Bi:NIG(x=1.0) are presented in Fig.3, respectively, and the average roughnesses Ra's of Bi:NIG (x=0-1.0) are summarized in Table 1. Relatively smooth surface is observed, though the surface of Bi:NIG(x=1.0) is slightly rougher reflecting the XRD signal. The Ra's of the order of 2-3 nm are obtained.

Figure 4 shows magnetization curves of the Bi:NIG(x=0-1.0) films on GGG(001) measured by vibrating sample magnetometer applying the magnetic field along the film plane. Clear hysteresis loops are observed in all the films. Nd^{3+} has the magnetic moment which is parallel to the magnetic moment of Fe^{3+} occupied tetrahedral sublattice. However, the difference of the saturation magnetization between the single-crystal NIG (159 emu/cc) and single-crystal YIG (139 emu/cc) is a little [15,16]. This can be attributed to a weak effective exchange field from Fe ions which acts upon the rare-earth sublattice in rare-earth iron garnets. On the other hand, in the Bi-substituted iron garnets, the presence of the Bi ions affects the indirect exchange interaction between the tetrahedral and octahedral sublattices and the Curie temperature becomes higher which leads to growth of the saturation magnetization at room

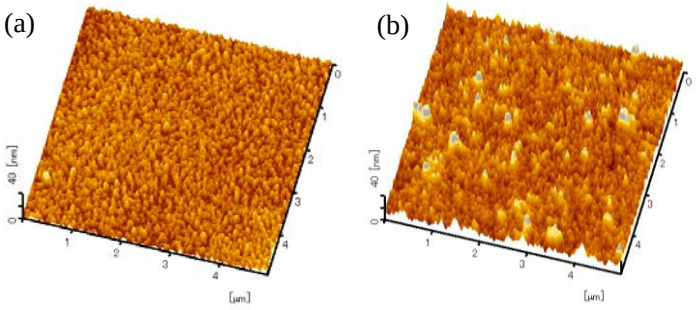

Fig.3 Topographic views of surface of (a) NIG and (b) Bi:NIG(x=1.0).

Table 1 Average roughness Ra of Bi:NIG (x=0-1.0) on GGG(001).

x	Ra [nm]
0	2.652
0.25	2.674
0.5	2.865
0.75	2.782
1.0	3.027

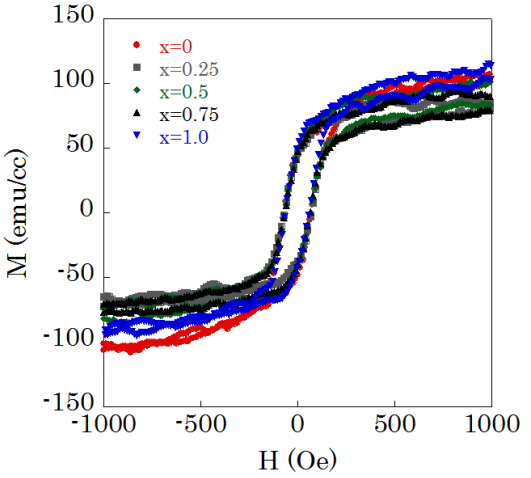

Fig.4 Magnetization curves of Bi:NIG(x=0-1.0) films on GGG(001) applying magnetic field along the film plane.

temperature[17]. The saturation magnetization of NIG in this experiment is small compared with the single-crystal value. The clear Bi composition dependence of the saturation magnetization is not observed.

The electric voltage V caused by the LSSE with ΔT=10 K were measured. Figure 5 shows (a) the magnetic field dependence of the voltage V for Bi:NIG(x=0-1.0)/Pt bilayers on GGG(001) and (b) the comparison between the LSSE voltage for NIG/Pt bilayer and the magnetization curve for NIG film. Clear hysteresis loops are observed in all the samples and the magnetic field dependence of LSSE voltage is in the good agreement with the magnetization curve. Bi composition dependences of (a) the amplitude of LSSE voltage V normalized by Pt length l and temperature difference ΔT and (b) the $V/\Delta T$ divided by Pt resistance R are plotted in Fig.6, respectively. It can be seen that the LSSE voltage increases with increasing Bi composition. Resistivity of Pt in the samples are similar ranging from

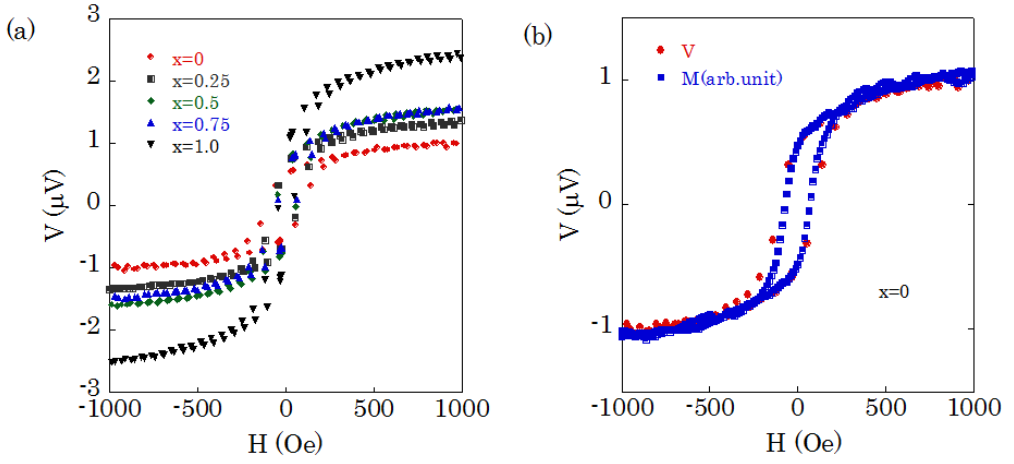

Fig5 (a) Magnetic field dependence of thermoelectric voltage V for Bi:NIG(x=0-1.0)/Pt bilayers on GGG(001) and (b) comparison between the LSSE voltage for NIG/Pt sample and the magnetization curve for NIG film.

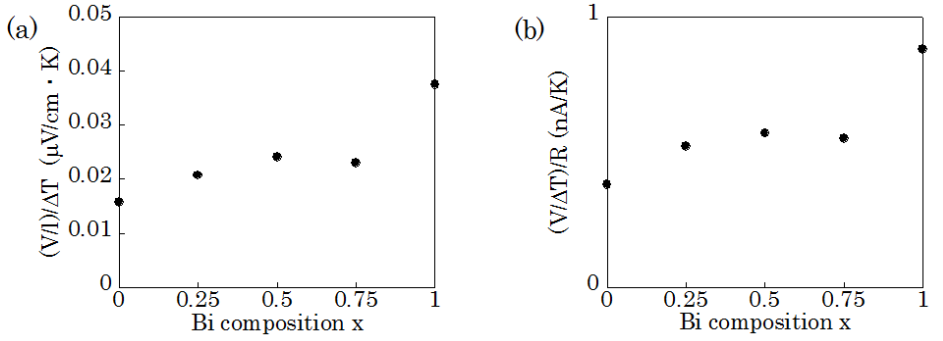

Fig.6 Bi composition dependences of (a) amplitude of LSSE voltage V normalized by Pt length l and temperature difference ΔT and (b) $V/\Delta T$ divided by Pt resistance R.

4.01×10^{-7} to 4.24×10^{-7} Ω·m. Therefore, the $(V/R)/\Delta T$ also indicates the same characteristics. Though the peak intensity of XRD signal and surface roughness for Bi:NIG do not improved compared with those for NIG as mentioned before, the amplitude of the LSSE voltage for Bi:NIG with x=1.0 is more than two times larger than that for NIG. The SSE voltage is dependent on the following three factors: the spin Hall angle, the difference of effective temperature between magnon and electron, and the spin mixing conductance at the interface [18]. In our case, it would be necessary to pay attention to the influence of magnetic moment of Nd^{3+} which changes by varying the Bi composition. Further experiments such as ferromagnetic resonance measurements to quantify the spin-mixing conductance are needed.

The NIG/Pt and Bi:NIG(x=1.0)/Pt bilayers were also prepared on (111) oriented GGG. Figure 7 presents (a) XRD patterns, (b) magnetization curves and (c) magnetic field dependence of

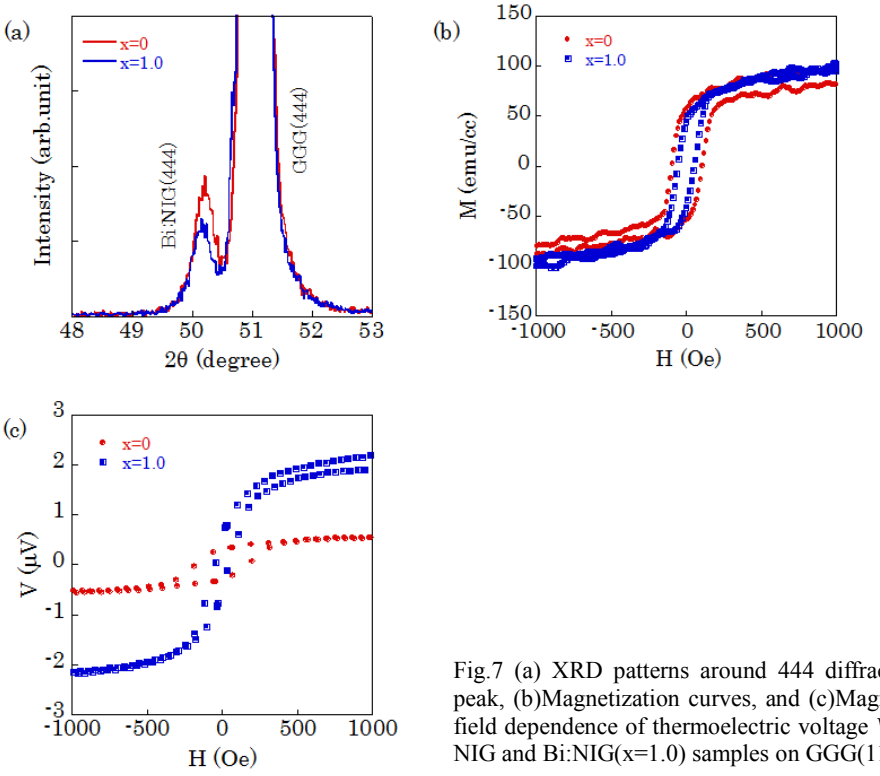

Fig.7 (a) XRD patterns around 444 diffraction peak, (b)Magnetization curves, and (c)Magnetic field dependence of thermoelectric voltage V for NIG and Bi:NIG(x=1.0) samples on GGG(111).

thermoelectric voltage V for them (ΔT=10 K). In Fig.7 (a) and (b), the peak intensities of XRD signal and the behavior of magnetization curves are about the same as those for the Bi:NIG films on GGG(001). As can be seen in Fig.7(c), though the amplitude of the LSSE signal for both the NIG/Pt and Bi:NIG(x=1.0)/Pt bilayers on GGG(111) are slightly small compared with those on GGG(001), the LSSE voltage for Bi:NIG(x=1.0) is also larger than that for NIG in the case of GGG(111).

4 Conclusions

Bi:NIG thin films with various Bi composition x=0-1.0 were prepared on GGG substrates by the MOD method in order to investigate the Bi composition dependence of the LSSE. All films on both the GGG(001) and GGG(111) are highly oriented. It is clarified that the LSSE voltage for Bi:NIG(x=0-1.0) on GGG(001) increases with increasing Bi in this composition range. The LSSE voltage for Bi:NIG with x=1 is also larger than that for NIG in the case of GGG(111).

Acknowledgments

This work was partly supported by Japan Society for the Promotion of Science (JSPS), Grant-in-Aid for Scientific Research (C: 24560376), and Electric Technology Research Foundation of Chugoku.

References

[1] K. Uchida, S. Takahashi, K. Harai, J. Ieda, W. Koshibae, K. Ando, S. Maekawa, E. Saitoh, Nature, **455**, 778 (2008).
[2] K. Uchida, J. Xiao, H. Adachi, J. Ohe, S. Takahashi, J. Ieda, T. Ota, Y. Kajiwara, H. Umezawa, H. Kawai, G. E. W. Bauer, S. Maekawa, E. Saitoh, Nature Mater, **9**, 894 (2010).
[3] K. Uchida, T. Nonaka, T. Ota, E. Saitoh, Appl. Phys. Lett., **97**, 262504 (2010).
[4] H. Adachi, J. Ohe, S. Takahashi, S. Maekawa, Phys. Rev. B, **83**, 094410 (2011).
[5] R. Ramos, T. Kikkawa, K. Uchida, H. Adachi, I. Lucas, M. H. Aguirre, P. Algarabel, L. Morellon, S. Maekawa, E. Saitoh, M. R. Ibarra, Appl. Phys. Lett., **102**, 072413 (2013).
[6] S. Bosu, Y. Sakuraba, K. Uchida, K. Saito, T. Ota, E. Saitoh, K. Takanashi, Phys. Rev. B, **83**, 224401 (2011).
[7] C. M. Jaworski, J. Yang, S. Mack, D. D. Awschalom, J. P. Heremants, R. G. Myers, Nature Mater, **9**, 898 (2010).
[8] D. Meier, T. Kuschel, L. Shen, A. Gupta, T. Kikkawa, K. Uchida, E. Saitoh, J.-M. Schmalhorst, G. Reiss, Phys. Rev. B, **87**, 054421 (2013).
[9] A. Kirihar, K. Uchida, Y. Kajikawa, M. Ishida, Y. Nakamura, T. Manako, E. Saitoh, S. Yorozu, Nature mater., **11**, 686 (2012).
[10] H. Asada, A. Kuwahara, N. Sakata, T. Ono, T. Ishibashi, A. Meguro, T. Hashinaka, K. Kishimoto, T. Koyanagi, .J. Appl. Phys., **117**, 17C724 (2015).
[11] T. Yoshida, K. Oishi, T. Nishi, T. Ishibashi, Eur. Phys. J. B Web of Conferences, **75**, 05009 (2014).
[12] G. Lou, T. Yoshida, T. Ishibashi, J. Appl. Phys., **117**, 17A749 (2015).
[13] Z. Qiu, D. Hou, K. Uchida, E. Saitoh, J. Phys. D: Appl. Phys., **48**, 164013 (2015).
[14] T. Ishibashi, A. Mizusama, M. Nagai, S. Shimizu, K.Sato, N. Togashi, T. Mogi, M. Houchido, H. Sano, K. Kuriyama, J. Appl. Phys., **97**, 013516 (2005).
[15] S. E. G. Slusky, et al., Phys. Rev.34, 7811 (1986).
[16] W. H. Von Aulock, Handbook of Microwave Ferrite Materials (Academic, London, 1965).

[17] A. K. Zvezdin, V. A. Kotov, *Modern Magnetooptics and Magnetooptical Materials* (Institute of Physics Publishing, Bristol and Philadelphia, 1997).
[18] K. Uchida, T. Nonaka, T. Kikkawa, Y. Kajiwara, E. Saitoh, Phys. Rev. B, **87**, 104412 (2013).